energies

MDPI

Article

Experimental Investigation of CO_2 Huff-and-Puff Enhanced Oil Recovery in Fractured Low-Permeability Reservoirs: Core-Scale to Pore-Scale

Fenglan Zhao, Changhe Yang *, Shijun Huang, Mingyang Yang, Haoyue Sun and Xinyang Chen

College of Petroleum Engineering, China University of Petroleum (Beijing), Beijing 102249, China; zhfl@cup.edu.cn (F.Z.); hshj@cup.edu.cn (S.H.); 15556138068@163.com (M.Y.); sunhy0130@163.com (H.S.); chenxinyang1129@163.com (X.C.)

* Correspondence: 2022210410@student.cup.edu.cn

Abstract: CO_2 huff-n-puff is regarded as an effective method to improve the recovery of low permeability and tight oil reservoirs. To understand the impact of CO_2 huff-n-puff on crude oil mobilization in tight reservoirs with different fracture scales, this study conducted CO_2 huff-n-puff nuclear magnetic resonance (NMR) and microscopic visualization experiments, focusing on how varying fracture apertures and densities affect the efficiency of the CO_2 huff-n-puff. The results show that in scenarios with a single fracture, larger fracture apertures significantly boost oil mobilization within the fracture and the surrounding matrix. For instance, increasing the aperture from 20 μm to 70 μm improved the recovery factor by 9.20%. In environments with multiple fractures, greater fracture density enhances reservoir connectivity, and increases the CO_2 sweep area, and the complex fracture model shows a 4.26% increase in matrix utilization compared to the simple fracture model. Notably, the improvement in recovery due to multi-scale fractures is most significant during the first two huff-and-puff cycles, with diminishing returns in subsequent cycles. Overall, increasing both fracture size and density effectively enhances crude oil mobilization in tight reservoirs. These findings provide valuable insights into improving the recovery efficiency of CO_2 huff-and-puff techniques in tight oil reservoirs.

Keywords: tight oil reservoir; CO_2 huff-and-puff; NMR; microscopic visualization experiment; fracture

Citation: Zhao, F.; Yang, C.; Huang, S.; Yang, M.; Sun, H.; Chen, X. Experimental Investigation of CO_2 Huff-and-Puff Enhanced Oil Recovery in Fractured Low-Permeability Reservoirs: Core-Scale to Pore-Scale. *Energies* **2024**, *17*, 6207. https://doi.org/10.3390/en17236207

Academic Editor: Dameng Liu

Received: 19 November 2024
Revised: 5 December 2024
Accepted: 7 December 2024
Published: 9 December 2024

1. Introduction

The development of ultra-low permeability and tight oil reservoirs in China holds considerable promise. However, these reservoirs often feature low pressure, numerous natural fractures, intricate pore structures, and significant heterogeneity. These factors make it challenging to achieve effective production increases through natural depletion methods, with primary recovery rates often falling below 10% [1–4]. To enhance recovery from tight reservoirs, various enhanced oil recovery (EOR) techniques have been employed, including water flooding, gas flooding, and chemical flooding. Among these, CO_2-EOR is one of the most effective techniques for tight oil reservoirs [5]. The significant interactions between crude oil and carbon dioxide—such as viscosity reduction, oil swelling, diffusion, extraction, and miscibility—make CO_2 injection particularly advantageous. However, in tight reservoirs with natural fractures, CO_2 injection may lead to gas channeling [6]. Studies have shown that CO_2 huff-n-puff is an effective approach to mitigating gas channeling in single-well operations [7], as it not only supplements reservoir energy and enhances oil recovery but also facilitates CO_2 utilization and geological sequestration [8–10]. The presence of fractures not only increases the contact area between CO_2 and crude oil but also provides convenient pathways for oil extraction.

Extensive research has been conducted on CO_2 huff-and-puff technology, especially concerning tight oil reservoirs [11–14]. Post-volumetric fracturing, hydraulic fractures

interact with natural fractures, creating a complex network that significantly impacts the effectiveness of CO_2 huff-and-puff processes [15–17]. Bai et al. [18] investigated the effect of fractures on the dynamics of CO_2 huff-and-puff, discovering that fractures notably improve recovery rates during the early and middle stages. Cao et al. [19] found that fractures, while increasing CO_2 channeling and reducing the sweep area, also aid in oil recovery from smaller pores. Li et al. [20] studied the role of fractures in CO_2 huff-and-puff efficiency across reservoirs with different permeabilities, indicating that fractures significantly boost initial oil production and recovery while reducing the effect of permeability on recovery rates. Huang et al. [21] examined the microscopic influence of fractures on oil movement in shale pores, finding that fractures significantly enhance oil recovery from both small and large pores. Li et al. [22] conducted experiments on fracture quantity's impact on CO_2 huff-and-puff recovery, showing that increased fracture numbers substantially boost oil recovery rates in tight cores, primarily during the first two cycles. Liu et al. [23] performed microscopic visualization experiments under high-temperature and high-pressure conditions, allowing real-time observation of CO_2 huff-and-puff processes and clarifying their underlying mechanisms. Zhao et al. [24] conducted similar experiments on CO_2 flooding, showing that in low-permeability reservoirs with well-developed fractures, the huff-and-puff method is notably more effective than displacement.

In recent years, methods for studying microscopic residual oil have primarily included nano-CT technology, nuclear magnetic resonance (NMR) technology, and microscopic simulation model technology. The advantage of CT technology is its ability to achieve three-dimensional observation. It quantitatively analyzes rock physical properties and images to obtain information on the distribution of fluid saturation within the core, providing a clear representation of the rock's pore structure [25,26]. NMR technology is typically used in displacement experiments with real cores, offering high precision in its measurements [27–29]. The combination of glass etching simulation models with microscopic image acquisition systems has enabled the visualization of microscale displacement dynamics, with its application being most prevalent in gas injection and water flooding experiments [30].

Research indicates that few studies have explored the impact of fractures on CO_2 huff-and-puff from a multi-scale perspective. Accurately characterizing multi-scale fractures is crucial for effectively simulating the CO_2 huff-and-puff process in fractured tight oil reservoirs. This study utilizes nuclear magnetic resonance (NMR) technology and a multi-scale fracture microscopic etching model, focusing on the Chang7 reservoir as a case study. NMR and microscopic visualization experiments were conducted to simulate CO_2 huff-and-puff processes in tight oil reservoirs affected by fractures. The research examines how different fracture apertures and densities impact the efficacy of CO_2 huff-and-puff under multi-scale fracture conditions. It also investigates the mobilization characteristics and the distribution of residual oil within matrix pores. Furthermore, it studies the seepage behaviors of oil and gas between the matrix and fractures, as well as variations in CO_2 sweep characteristics and mobilization levels. These findings provide theoretical insights for advancing CO_2 huff-and-puff techniques in tight oil reservoirs.

2. Materials and Methods

2.1. Materials

(1) Oil and gas samples

In this study, the oil sample used was dead oil collected from the Chang7 member of the Changqing oil field. The characteristics of this oil are detailed in Figure 1. At the testing temperature of 75 °C, the oil sample has a viscosity of 2.15 mpa·s and a density of 0.747 g/cm^3. Its composition includes 56.31% saturated fraction, 11.28% aromatic fraction, 1.52% colloidal fraction, and 0.3% asphaltenes. The experimental gas used was CO_2 with a high purity of 99.9%, supplied by the Huatong Jingke Gas Company in China. The minimum miscibility pressure (MMP) between the CO_2 and the crude oil was determined to be 17.6 MPa at 75 °C. Based on field data, the oil recovery efficiency for different drive

mechanisms is presented in Figure 2. It is evident that carbon dioxide injection offers favorable economic benefits. Due to the rapid decline in reservoir pressure observed in the field, the experiments were conducted under immiscible conditions, aligning with the field situation, meaning the pressure was kept below the MMP to reflect realistic operational conditions in the reservoir. This approach allows researchers to study how CO_2 interacts with the oil under conditions that are representative of actual reservoir environments, offering insights into optimizing the CO_2 huff-and-puff process for improved oil recovery.

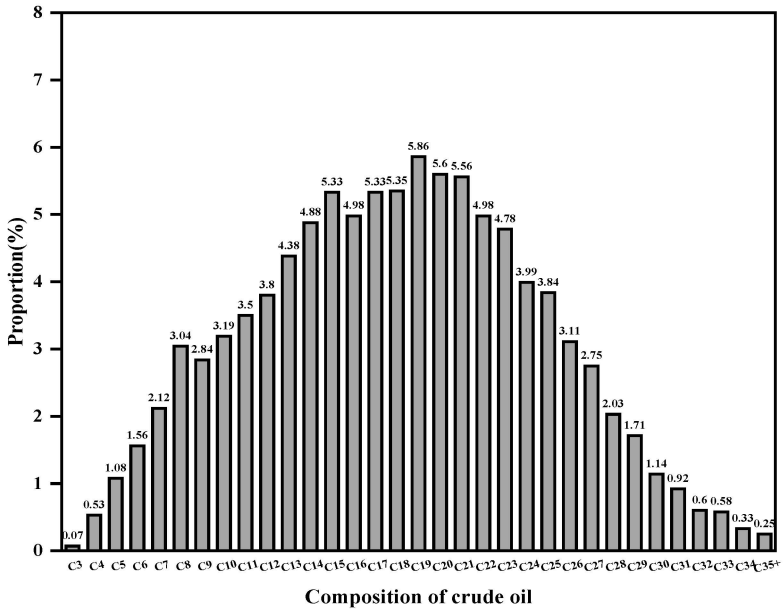

Figure 1. Compositional analysis of the crude oil.

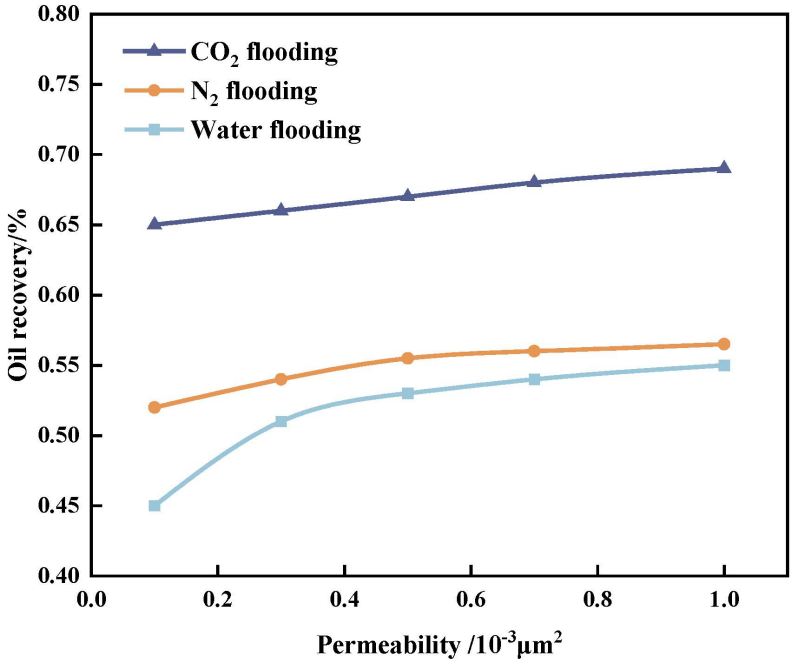

Figure 2. The oil recovery efficiency of different drive mechanisms.

(2) Cores

Core samples with comparable permeabilities and porosities were utilized, all sourced from the same tight oil reservoir. These core samples featured artificial cracks oriented along the axial direction. To simulate the effects of varying crack apertures, gaskets of

differing thicknesses were inserted into the core cracks. All cracks were positioned centrally within the cores to maintain consistency across experiments. These experimental setups were designed to assess how variations in fracture aperture impact the CO_2 huff-and-puff process, allowing for a detailed analysis of fluid flow and oil recovery under controlled conditions. The key parameters of the core samples, such as porosity, permeability, and other pertinent properties, are outlined in Table 1.

Table 1. The basic properties of core samples used in the experiments.

Core Number	Length/cm	Diameter/cm	Porosity/%	Permeability/ 10^{-3} μm^2	Fracture Aperture/μm
1	7.24	2.54	10.36	0.094	20
2	7.31	2.52	10.54	0.089	50
3	7.26	2.54	10.12	0.093	70

(3) Etched glass models

The matrix pores were initially described based on thin sections of the reservoir core casts. After this, fractures of various scales were incorporated into the model. The microscopic visualization model had an overall size of 10 × 10 cm, with an etched area measuring 8 × 8 cm. Within this etched region, matrix pores and fractures of different sizes were randomly distributed. The fractures featured apertures of 1000 μm, 100 μm, and 50 μm, allowing for the examination of various fracture scales and their effects on fluid flow and oil recovery. Based on the fracture density, the model was divided into two categories: a simple fracture model and a complex fracture model, as illustrated in Figure 3.

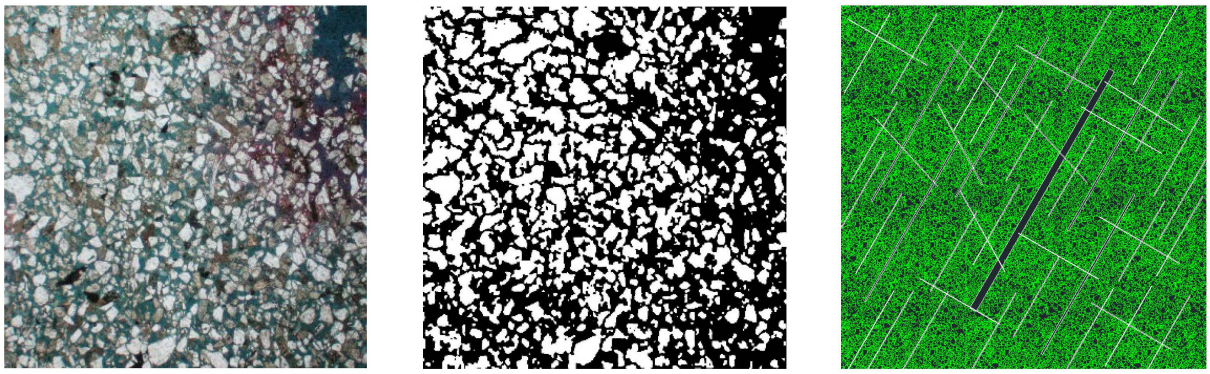

Figure 3. Glass etching model fabrication process: (**a**) cast sheet; (**b**) binarization process; and (**c**) CAD model.

2.2. Apparatus

The experimental setup utilized a range of specialized equipment to conduct the study. Key devices included: ISCO double cylinder pump, intermediate container (500 mL, pressure 50 MPa), core gripper (maximum pressure of 70 MPa, The maximum temperature is 150 °C), high-power microscope, constant temperature and constant pressure micro model gripper, display, confining pressure pump, back pressure pump, thermostat, a low field MesoMR12-150H NMR system manufactured by the Niumag Corporation Ltd. in Suzhou, China (magnetic field intensity is 0.3 ± 0.05 T, instrument main frequency is 1 MHz). High precision syringe pump (model 100DX, Jiangsu Hai'an Research Instrument Co., Ltd., Nantong, China, injection accuracy 0.001–6 mL/min), VHX6000 microscope (Keyence, Osaka, Japan, 15–50 frames/s).

2.3. Experimental Procedure

2.3.1. CO_2 Huff-and-Puff Experiment for Low-Permeability Cores

Figure 4 shows the experimental setup for CO_2 huff-and-puff. It is important to note that all experiments were conducted under immiscible conditions. The specific experimental steps are outlined as follows:

(1) Dry core measurement: Choose experimental cores, clean and dry them, and then weigh the dry core. Measure its length and diameter to calculate the core volume.
(2) Oil saturation: Dry the core in a 96 °C oven for 10 h. Once cooled, saturate it with crude oil under vacuum, then age it at 75 °C and 10 MPa for 48 h. Perform an NMR scan on the aged core.
(3) Injection stage: Position the core in a core holder, injecting CO_2 at 0.2 mL/min. Keep the confining pressure 3–5 MPa above the upstream pressure, and stop when the injection pressure stabilizes at 10 MPa.
(4) Soaking stage: Close the core holder's inlet and outlet valves and soak for 5 h.
(5) Production Stage: Following soaking, open the injection end valve and gradually reduce the back pressure to let CO_2 carry out the crude oil. Stop when oil production ceases.
(6) Repeat the injection, soaking, and production stages (steps 3 to 5) for a total of four cycles to complete the huff-and-puff process.

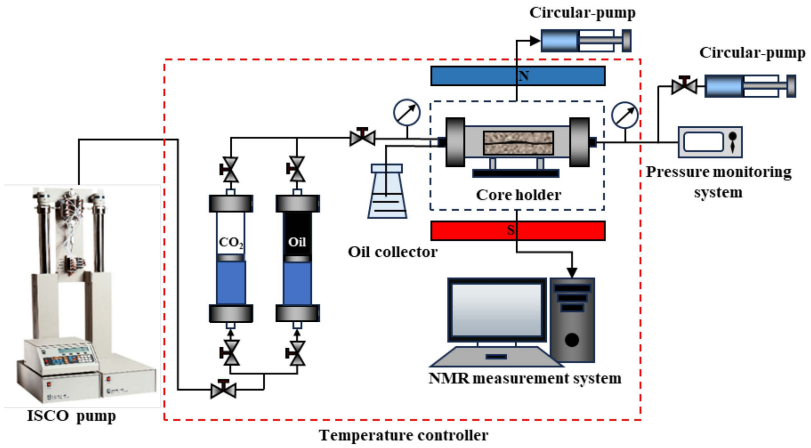

Figure 4. Experimental equipment for CO_2 injection.

2.3.2. Microscopic Non-Miscible CO_2 Huff-and-Puff Experiment

Figure 5 shows the experimental equipment of microscopic visualization, which was conducted under immiscible conditions. The specific experimental steps are as follows:

(1) Model cleaning: Inject petroleum ether into the glass-etched model at 20 μL/min. Once cleaned, place the model in a 96 °C oven to dry for 24 h.
(2) Oil saturation: Place the etched model in a micro-model holder and apply a vacuum at room temperature (23 °C) for one hour. Then, saturate the model with oil at 20 μL/min until 99.9% of the pores are filled with crude oil.
(3) Injection stage: Start by opening the microscope camera and adjusting the focus for a clear image. Begin recording, set the back pressure to 0.1 MPa, and use the confining pressure pump to maintain a pressure of 0.3 to 0.5 MPa above the model pressure. Set the injection rate to 30 μL/min and close the inlet valve when the injection pressure reaches 0.5 MPa.
(4) Soaking stage: Keep the inlet valve closed and let the system soak for 20 min.
(5) Production stage: Open the inlet valve to allow the pressure in the model to gradually drop to atmospheric pressure. Record the entire oil extraction process, capturing all stages. Stop recording when oil extraction ceases.
(6) Repeat the injection, soaking, and production stages (steps 3 to 5) for a total of four cycles to complete the huff-and-puff process.

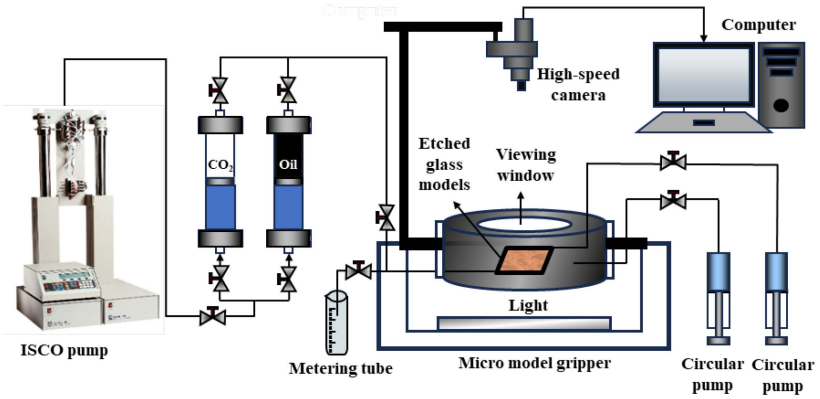

Figure 5. Experimental equipment of microscopic visualization.

2.4. Principle of Low Field Nuclear Magnetic Resonance (NMR)

The transverse relaxation time (T_2) of fluid NMR in porous media is mainly composed of three parts: surface relaxation time (T_2, surface), bulk relaxation time (T_2, bulk), and diffusion relaxation time (T_2, diffusion) [31–33]:

$$T_2 = \frac{1}{T_{2,\text{surface}}} + \frac{1}{T_{2,bulk}} + \frac{1}{T_{2,\text{diffusion}}} \tag{1}$$

where T_2 surface is the surface relaxation time; T_2 bulk is the bulk relaxation time; and T_2 diffusion is the diffusion relaxation time, respectively. Because the uniform magnetic field and the bulk relaxation time are much greater than T_2, T_2 bulk and T_2 diffusion are usually neglected. Thus, T_2 can be expressed as follows [34]:

$$T_2 = T_{2,surface} = \frac{V}{\rho_t S} \tag{2}$$

where ρ_t is the surface relaxivity, m/ms; S is the surface area, μm^2; and V is the pore volume, μm^3.

If the pore structure is simplified as a standard spherical structure or a columnar structure, the ratio of the surface area to the volume can be expressed as follows:

$$\frac{S}{V} = \frac{F_s}{r} \tag{3}$$

where F_s is the shape factor of a pore, and r is the pore radius, μm.

Combining Equations (2) and (3), we can obtain the following:

$$T_2 = T_{2,surface} = \frac{r}{\rho_t F_s} \tag{4}$$

According to Equation (4), T_2 is proportional to r, that is, T_2 can reflect the size of r, and the signal intensity can reflect the amount of crude oil in the corresponding different aperture. Therefore, the amount of crude oil in the core and the degree of recovery can be calculated according to the distribution of the T_2 spectrum at different stages, as follows:

$$Q_t = \int_{t_0}^{t_s} A_t dt \tag{5}$$

$$E_r = \frac{Q_2 - Q_1}{Q_0} \times 100\% \tag{6}$$

In Equation (6), Q_t is the crude oil stock at time t, t_0 is the initial transverse relaxation time corresponding to the T_2 spectral curve at time t, ms; T_S is the termination transverse

relaxation time corresponding to the T_2 spectral curve at time T, ms; A_t is the signal intensity corresponding to the T_2 spectral curve; E_r is the oil recovery degree from time t_1 to time t_2, %; Q_0, Q_1 and Q_2 are the crude oil stocks corresponding to the initial saturation times, t_1 and t_2, respectively.

3. Results and Discussion

3.1. Characteristics of Crude Oil Mobilization During CO_2 Huff-n-Puff

3.1.1. Microscopic Characteristics of Crude Oil Mobilization

Figure 6 illustrates the NMR spectra of saturated oil core samples. Previously, a power law relationship between NMR relaxation time and pore radius was described. In earlier studies, the conversion relationship between NMR relaxation time and pore radius was determined as [35,36]:

$$R = 0.0068T_2^{0.4237} \quad (7)$$

By applying the conversion equation to NMR relaxation times, we can determine the pore distribution of the core. Figure 6 illustrates the oil recovery characteristics of core sample 1 under different cycles. It is clear that the T_2 spectra of oil-saturated cores show a bimodal pattern, with the right peak significantly higher than the left. This indicates that the experimental cores have well-developed macropores, while micropores and nanopores are less developed. Comparing the signal distribution of T_2 curves across different cycles helps delineate the distribution of the matrix and fractures: T_2 values between 0.1 ms and 500.0 ms correspond to the core matrix, while values between 500.0 ms and 10,000.0 ms correspond to fractures. Based on related literature and NMR principles, pore types in the matrix can be further classified according to the characteristics of the T_2 curve valleys: pores with T_2 values from 0.1 ms to 10.0 ms are identified as small pores, and those with T_2 values from 10.0 ms to 500.0 ms are identified as large pores.

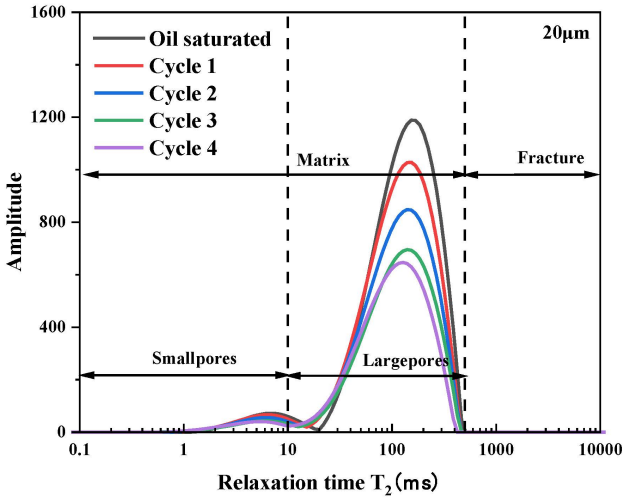

Figure 6. NMR T_2 spectra of core no. 1 samples during CO_2 huff-n-puff.

Figures 7 and 8 respectively show the oil recovery characteristics of core sample 2 and core sample 3 under different cycles. As fracture aperture increases, the decline in crude oil signal amplitude is significantly greater during the first two cycles, notably affecting large pores (20.0 ms $\leq T_2 \leq$ 431.0 ms) and, to a lesser extent, some small pores (1.0 ms $\leq T_2 \leq$ 7.0 ms). This is because larger fracture apertures enhance the flow capacity, allowing CO_2 to diffuse into the matrix during the soaking period and dissolve in the oil. During extraction, fractures act as flow channels, reducing resistance and enabling oil in the matrix to expand into the fractures for more efficient extraction. As the number of huff-and-puff cycles increases, the degree of oil extraction significantly decreases after the third cycle. Oil movement primarily occurs through pores with relaxation times between 7.0 ms and 20.0 ms, into some small (1.0 ms $\leq T_2 \leq$ 7.0 ms) and large pores (20.0 ms $\leq T_2 \leq$ 170.0 ms).

By this stage, oil near fractures has been extracted, while oil farther away is harder to extract due to slow molecular diffusion and high flow resistance in the matrix. With the increase of fracture aperture, the lower limit of effective pore utilization decreases. This is because larger apertures allow greater CO_2 injection volumes and contact areas, enhancing molecular diffusion. Early extraction of more oil creates favorable conditions for subsequent CO_2 contact with oil in smaller pores.

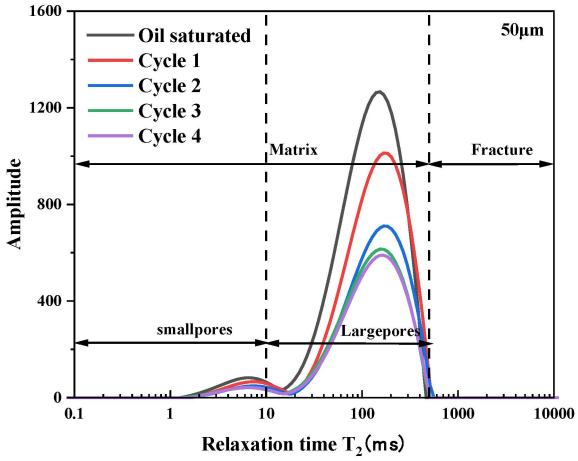

Figure 7. NMR T_2 spectra of core no. 2 samples during CO_2 huff-n-puff.

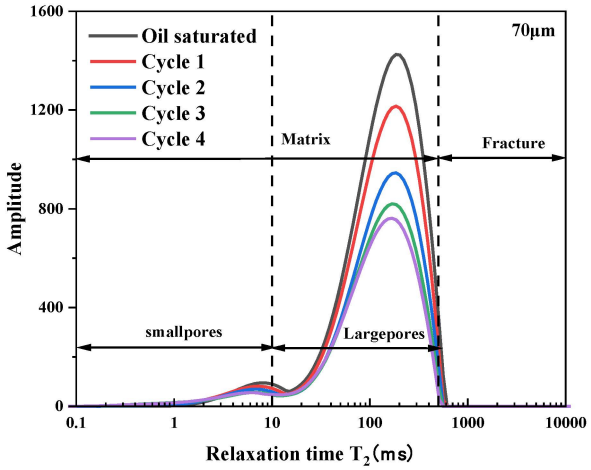

Figure 8. NMR T_2 spectra of core no. 3 samples during CO_2 huff-n-puff.

3.1.2. Micro-Characteristics of Crude Oil Mobilization

Figure 9 illustrates the variation in oil recovery degree for different cores in each cycle, combined with NMR analysis. The results show that in the first cycle, the oil recovery for fracture apertures of 20 μm, 50 μm, and 70 μm are 14.29%, 17.29%, and 22.82%, respectively. The highest recovery occurs in the fourth cycle, but the recovery degree gradually decreases in subsequent cycles. As the fracture opening increases, the recovery degree in the same cycle also increases; however, the most significant gains occur in the first two cycles, with diminishing returns in later cycles. Comparing the cumulative oil recovery degrees for different fracture apertures (Figure 10), the recovery degrees after four cycles are 43.73% for 20 μm, 47.81% for 50 μm, and 52.93% for 70 μm. The utilization degrees for cores with 50 μm and 70 μm fracture apertures are 4.08% and 9.20% higher than for those with 20 μm apertures. This indicates that larger fracture apertures expand the effective percolation channels, enhancing crude oil recovery. The increase in fracture opening contributes to recovery in two ways: it increases the contact area between CO_2 and crude oil, and it

significantly reduces the counterflow resistance of crude oil during the recovery stage, aiding in more efficient oil extraction.

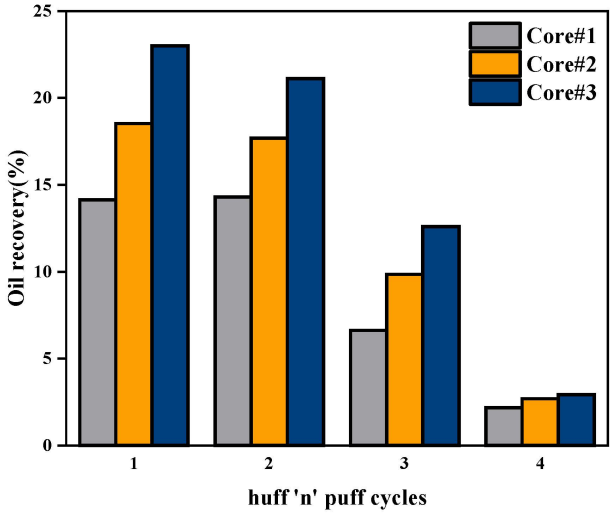

Figure 9. Variation in oil recovery degree for core samples in each cycle.

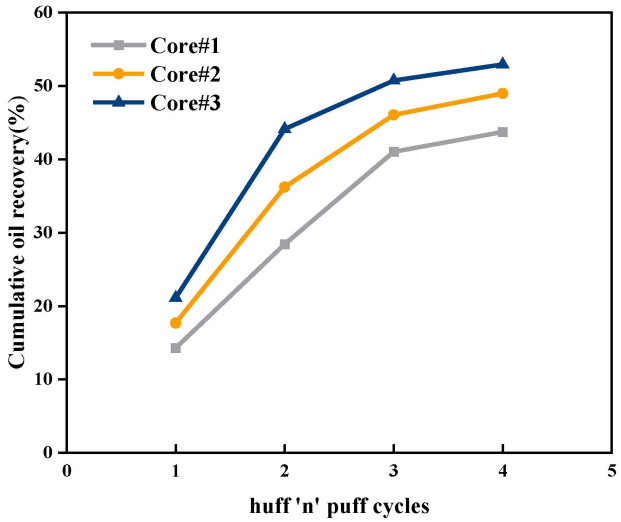

Figure 10. Cumulative oil recovery for core samples with different fracture apertures.

3.2. Distribution Characteristics of Residual Oil After CO_2 Huff-and-Puff

Figure 11 displays NMR images showing the remaining oil in each cycle for different cores. In these images, the red shaded areas indicate high oil saturation, and the left side marks the injection and production end. Initially, the saturated core has a relatively uniform oil saturation distribution. However, after CO_2 throughput, oil saturation significantly decreases at the injection and production end, while remaining relatively high at the distal end. When fractures are present, they serve as effective percolation channels, enhancing the contact between CO_2 and the matrix oil. During the injection and socking phase, CO_2 diffuses through the fractures into matrix pores, pushing the crude oil towards the distal end and connecting the surrounding matrix pores. In the production stage, as CO_2 fully interacts with the crude oil in the matrix pores, the pressure differential generates negative convection, causing the crude oil to flow in reverse from the matrix to the fractures for extraction, primarily affecting oil near the injection end and lessening influence on distal oil. When fracture apertures are 20 μm, the remaining oil is mainly found at both ends of the core. As the throughput cycles increase, the remaining oil at the outlet decreases, while more oil remains further from the outlet, with minimal fracture channel and gravity effects.

With larger fracture apertures (50 μm and 70 μm), the negative convection phenomenon becomes more pronounced, leading to a reduction in the remaining oil within the cyclic fracture channels. As the huff-and-puff cycle increases, the remaining oil at the distal end decreases, pressure propagates effectively, the distance influenced by CO_2 injection increases, and gravity effects become more pronounced.

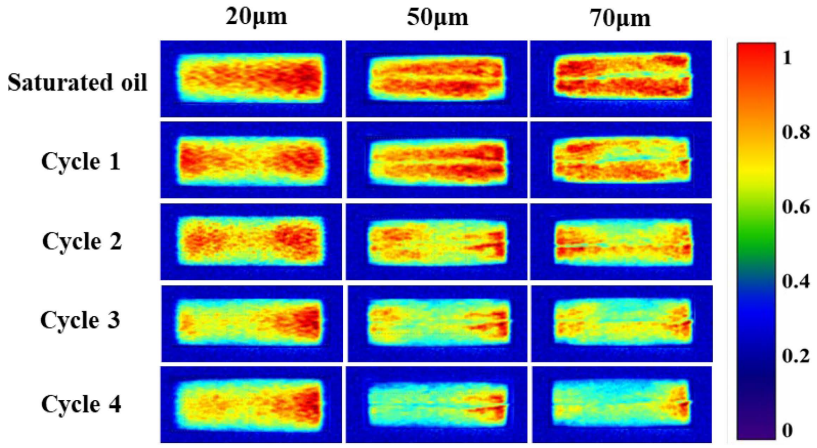

Figure 11. NMR images of the oil-saturated sample and after CO_2 huff-and-puff.

3.3. Characteristics of Oil and Gas Percolation Changes and Sweep Efficiency

3.3.1. Percolation Variation Between Oil and Gas

Figure 12 illustrates the characteristics of oil and gas percolation across different cycles using the simple fracture model. The white areas represent the CO_2 spread area, and the oil–gas interface is distinct. During the gas injection period, fractures act as primary flow channels, with CO_2 preferentially entering due to velocity potential. The flow is dominated by large-scale and mesoscale fractures. Initially, the gas displacement front forms a finger-like pattern. As the huff-and-puff cycle increases, CO_2 concentration redistributes, becoming higher in areas with better pore connectivity. Diffusion mainly occurs along fractures parallel to the main diagonal, gradually widening the finger-like spread.

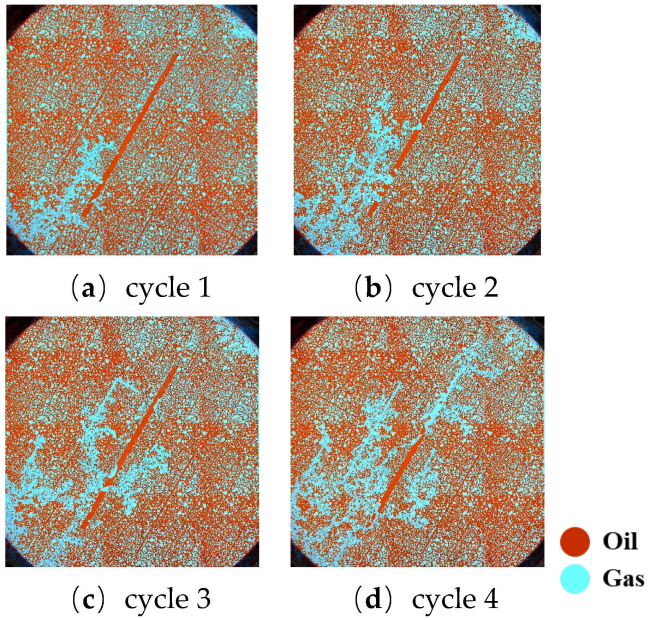

Figure 12. The oil and gas seepage characteristics of simple fracture model.

Figure 13 illustrates the characteristics of oil and gas percolation across different cycles using the complex fracture model. The percolation primarily occurs through connected fractures, with a noticeable channeling effect. During injection, CO_2 moves from one fracture to adjacent ones, migrating into previously unaffected areas through well-connected channels. It replaces the oil in the matrix pores and enters the fractures. During the production period, some crude oil remains trapped in distant pores and fractures due to the long reverse flow path. As subsequent injections occur, channeling increases and a new gas displacement path develops. Compared to the simple fracture model, the increased fracture density in the complex model enhances overall connectivity, significantly expanding the propagation area on both sides of the main diagonal, and demonstrating network propagation characteristics.

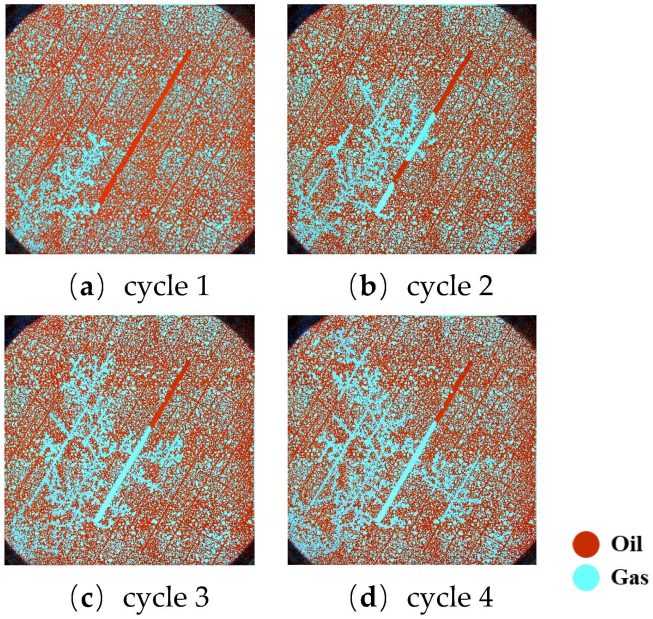

Figure 13. The oil and gas seepage characteristics of complex fracture model.

3.3.2. Sweep Efficiency Characteristics

Figure 14 presents the experimental results of amplitude change features that have been binarized using ImageJ software (v1.54) for different models. The wave area for the first cycles was found to be 5.72% and 6.43%, respectively. Since CO_2 had limited exposure to the cracks, it primarily diffused through the matrix under pressure difference, resulting in a minimal difference. As throughput cycles increased, the spread range gradually expanded; however, the rate of increase decreased progressively. In the simple fracture model, the spread areas for the second to fourth huff-and-puff cycles were measured at 11.07%, 16.03%, and 21.52%, respectively. In contrast, for the complex fracture model, the spread areas were recorded at 15.19%, 23.73%, and 30.55%. Compared to the simple fracture model, the complex fracture model showed an increased spread range under similar huff-and-puff conditions. From the first to the third cycle, the spread range increased by 4.11%, 7.69%, and 9.03%, respectively. This demonstrates that higher fracture density significantly enhances the CO_2 spread range, thereby improving the energy replenishment effect.

Figure 15 compares the maximum sweep distances observed in the fourth cycle. The previous injection cycle significantly affects the outcomes of subsequent cycles, and this impact is even more pronounced in the presence of induced fractures. Although the injection direction aligns with the diagonal, it deviates slightly from most fracture orientations, indicating that fracture direction affects the spread area in a remarkable way. In the simple fracture model, the wave front extends along the main diagonal, reaching a maximum of 11.361 cm. Poor connectivity results in a shorter wave front along the secondary diagonal, with a maximum distance of 5.946 cm. In the complex fracture model, after spreading 7.568 cm longitudinally—a reduction of 50%—the wave redirects along the

secondary diagonal via conjugate fractures, reaching up to 9.408 cm, an increase of 58%. This configuration significantly enhances the overall spread range and reduces resistance to crude oil flow, mitigating the negative effects of gas breakthroughs.

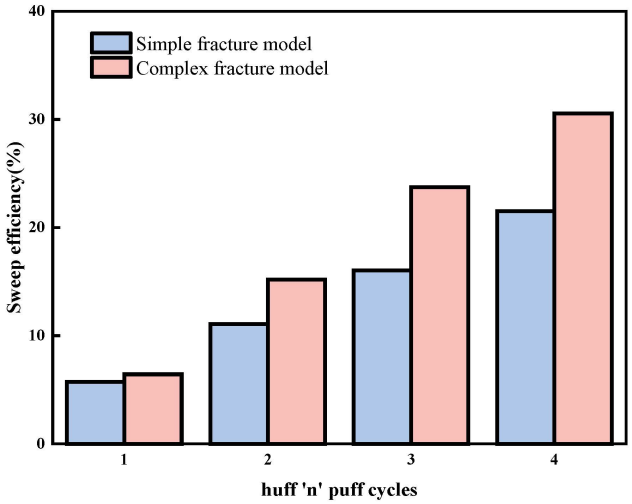

Figure 14. The sweep range of different models after CO_2 huff-and-puff.

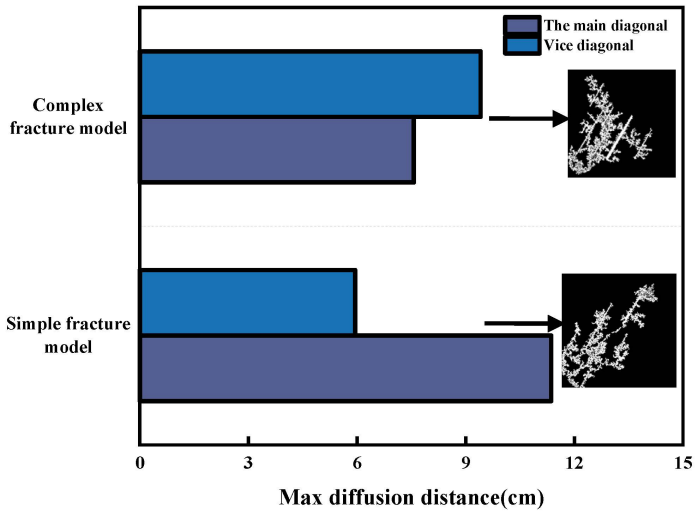

Figure 15. The maximum sweep distance in the fourth round for different models.

3.4. Comparison of Enhanced Oil Recovery Effects

Figure 16 illustrates the extent of fracture-matrix utilization under different CO_2 huff-and-puff cycles, highlighting that the reticular fracture model consistently surpasses the single fracture model in extraction efficiency. Across equivalent huff-and-puff cycles, the complex fracture model exhibits superior matrix utilization compared to the simple fracture model. Initially, increasing fracture density significantly enhances oil recovery in the first two CO_2 huff-and-puff cycles; however, this advantage decreases in later cycles. By the fourth cycle, matrix utilization in the complex fracture model is 4.6% higher than in the simple model. During both the injection and soaking phases, CO_2 primarily disperses through mesoscale fractures, then microscale fractures, with matrix pores being utilized last. During the production phase, crude oil flows counter-currently along dominant pathways, with large-scale fractures serving as primary seepage channels and storage reservoirs. As the huff-and-puff cycles advance, the utilization rates across different fracture scales gradually rise. Crude oil mobilization is particularly effective within mesoscale fractures and their adjacent matrices. Notably, in earlier stages, microscale fractures show higher utilization

than large-scale ones across various models, especially in complex configurations. However, by the fourth cycle, this trend reverses: large-scale fractures exhibit greater mobilization than microscale fractures. Additionally, there is a 4.26% increase in mobilization within simple models at this point. Consequently, during production, large-scale fractures become the principal drainage pathways for crude oil, indicating a flow trajectory that starts in the matrix, moves through large-scale fractures, and transitions through medium- to small-scale structures toward the production endpoints.

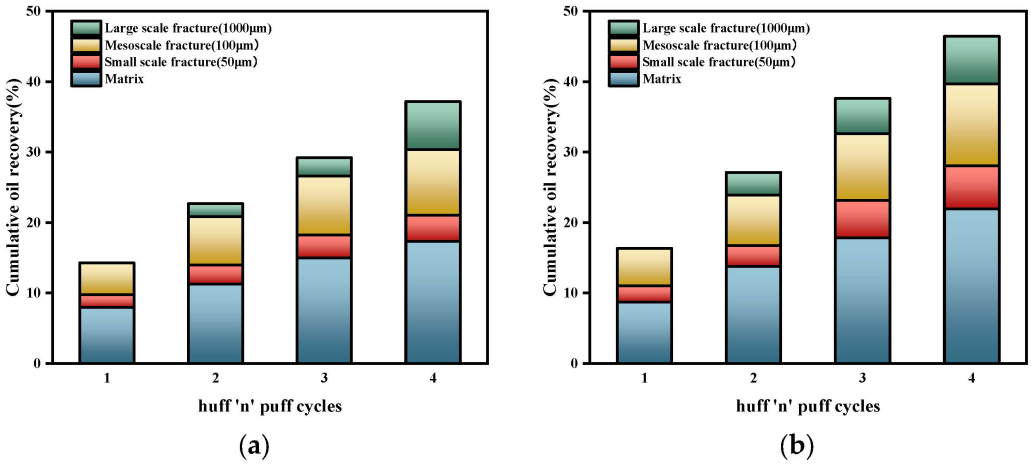

Figure 16. The extent of fracture-matrix utilization under different CO_2 huff-and-puff cycles: (**a**) simple fracture model; and (**b**) complex fracture model.

4. Conclusions

The CO_2 huff-n-puff experiments and microscopic visualization offer insights into crude oil mobilization in tight reservoirs under different fracture conditions. Key conclusions are as follows:

(1) The increase in fracture aperture enhances CO_2 and crude oil interaction during injection and soaking stages, improving oil mobilization within the matrix. Larger apertures reduce the threshold for mobilizing oil from matrix pores, with most oil mobilized from large pores, while recovery from smaller pores remains limited.

(2) Increasing fracture density improves oil discharge areas. Induced fractures have a significant impact on CO_2 diffusion. Multi-scale fractures predominantly enhance recovery in medium and small-scale fractures and adjacent matrices, while large-scale fractures serve as major flow channels. Benefits are most significant in the first two cycles, with diminishing effects in later cycles.

(3) Multi-scale fractures can significantly enhance the negative convection effect, leading to a substantial reduction of residual oil both near and far from the injection point. The spatial distribution of residual oil demonstrates the movement of crude oil from the matrix to fractures and then to the production endpoint during the huff-n-puff process.

Finally, we will further expand the scope of our research to consider the limits of effective utilization of tight oil reservoirs in the presence of complex fractures. Additionally, we will consider the impact of dynamic soaking time on recovery rates in our future work.

Author Contributions: Conceptualization, F.Z.; methodology, F.Z.; validation, C.Y.; formal analysis, S.H.; investigation, S.H.; data curation, M.Y.; writing—original draft preparation, C.Y.; writing—review and editing, H.S. and X.C.; visualization, C.Y.; supervision, S.H. All authors have read and agreed to the published version of the manuscript.

Funding: This research was supported by the National Natural Science Foundation of China (no. 52174039); and the China Petroleum Strategic Cooperation Technology Special Project (no. ZLZX2020−02−04).

Data Availability Statement: The authors confirm that the data supporting the findings of this study are available within the article.

Conflicts of Interest: The authors declare no conflicts of interest.

References

1. Zhao, J.Z. Concepts, classification, and resource potential of unconventional oil and gas. *Nat. Gas Geosci.* **2012**, *23*, 393–406.
2. Yu, F.W.; Su, H. Exploration of characteristics and development strategies for tight oil in China. *Contemp. Chem. Ind.* **2015**, *44*, 1550–1552.
3. Zhu, W.Y.; Yue, M.; Liu, Y.F.; Liu, K.; Song, Z.Y. Advances in the development theory of tight oil reservoirs in China. *Chin. J. Eng.* **2019**, *41*, 1103–1114.
4. Li, G.X.; Zhu, R.K. The development status, challenges, and issues of concern for unconventional oil and gas in China. *China Pet. Explor.* **2020**, *25*, 1–13.
5. Zuloaga, P.; Yu, W.; Miao, J.; Sepehrnoori, K. Performance evaluation of CO_2 Huff-n-Puff and continuous CO_2 injection in tight oil reservoirs. *Energy* **2017**, *134*, 181–192. [CrossRef]
6. Matter, J.M.; Stute, M.; Snæbjörnsdottir, S.Ó.; Oelkers, E.H.; Gislason, S.R.; Aradottir, E.S.; Sigfusson, B.; Gunnarsson, I.; Sigurdardottir, H.; Gunnlaugsson, E.; et al. Rapid carbon mineralization for permanent disposal of anthropogenic carbon dioxide emissions. *Science* **2016**, *352*, 1312–1314. [CrossRef]
7. Bikkina, P.; Wan, J.; Kim, Y.; Kneafsey, T.J.; Tokunaga, T.K. Influence of wettability and permeability heterogeneity on miscible CO_2 flooding efficiency. *Fuel* **2016**, *166*, 219–226. [CrossRef]
8. Qian, Y.; Li, Y.; Wang, X.; Zhang, H.; Wang, T.; Zhu, S.; Zhou, H.; Zhang, H.; Liu, Z. Study on energy supplement strategy of carbon dioxide huff and puff in horizontal well of tight oil sandstone reservoir. In Proceedings of the 2022 Global Conference on Robotics, Artificial Intelligence and Information Technology, Chicago, IL, USA, 30–31 July 2022; pp. 787–789.
9. Kang, W.; Zhou, B.; Issakhov, M.; Gabdullin, M. Advances in enhanced oil recovery technologies for low permeability reservoirs. *Pet. Sci.* **2022**, *19*, 1622–1640. [CrossRef]
10. Hu, Y.L.; Hao, M.Q.; Chen, G.L.; Sun, R.Y.; Li, S. CO_2 enhanced oil recovery and sequestration technology and practice in China. *Pet. Explor. Dev.* **2019**, *46*, 716–727. [CrossRef]
11. Zhan, F.; Song, K.P.; Shang, W.T.; Yang, E.L.; Liu, L. Research on the Optimal Parameters of CO_2 Huff and Puff for a Single Well in Low Permeability Reservoirs. *Spec. Oil Gas Reserv.* **2010**, *17*, 70–72+131.
12. Huang, X.L.; Jia, X.F.; Zhou, X.; Zheng, S.P.; Yan, W.D.; Yuan, Y.Z. Optimization of CO_2 Huff and Puff Parameters for Long Cores in Low Permeability Reservoirs of the Yanchi Oilfield. *Xinjiang Pet. Geol.* **2015**, *36*, 313–316.
13. Tang, X.; Li, Y.; Han, X.; Zhou, Y.; Zhan, J.; Xu, M.; Zhou, R.; Cui, K.; Chen, X.; Wang, L. Dynamic characteristics and influencing factors of CO_2 huff and puff in tight oil reservoirs. *Pet. Explor. Dev.* **2021**, *48*, 817–824. [CrossRef]
14. Shi, Y.; Wu, B.; Wang, H.; Li, Y.; Liu, Z.; Xu, C.; Qin, J.; Li, Y.; Song, Z.; Liu, H. Insights into CO_2 huff-n-puff mechanisms from laboratory experiment and single-well pilot test in the Lucaogou tight oil reservoir, Jimsar sag, China. *Geoenergy Sci. Eng.* **2024**, *232*, 212456. [CrossRef]
15. Li, Y.; Zhu, Y.W.; Li, Z.Y.; Jiang, T.X.; Xue, Z.J.; Shen, Z.Q.; Xiao, P.F.; Yu, H.M.; Chen, Z.Y.; Zhao, Q.M.; et al. CO_2 Injection Development Technology for Shale Oil in Jiyang Depression. *Pet. Explor. Dev.* **2024**, *51*, 855–864. [CrossRef]
16. Kang, Y.L.; Tian, J.; Luo, P.Y.; You, L.J.; Liu, X.F. Technical bottlenecks and development strategies for enhancing oil recovery in tight oil reservoirs. *Acta Pet. Sin.* **2020**, *41*, 467–477.
17. Wang, W.D.; Zhao, G.Y.; Su, Y.L.; Feng, Z.T. Application of volume fracturing technology in tight oil reservoirs. *Xinjiang Pet. Geol.* **2013**, *34*, 345–348.
18. Bai, H.; Zhang, Q.; Li, Z.; Li, B.; Zhu, D.; Zhang, L.; Lv, G. Effect of fracture on production characteristics and oil distribution during CO_2 huff-n-puff under tight and low-permeability conditions. *Fuel* **2019**, *246*, 117–125. [CrossRef]
19. Cao, A.; Li, Z.; Zheng, L.; Bai, H.; Zhu, D.; Li, B. Nuclear magnetic resonance study of CO_2 flooding in tight oil reservoirs: Effects of matrix permeability and fracture. *Geoenergy Sci. Eng.* **2023**, *225*, 211692. [CrossRef]
20. Li, F.X.; Wang, H.B.; Zhou, T.; Han, L. Impact of Fractures on CO_2 Huff and Puff Performance and Pore Utilization Characteristics in Shale Oil Reservoirs. *Pet. Drill. Tech.* **2022**, *50*, 38–44.
21. Huang, X.; Li, X.; Zhang, Y.; Li, T.T.; Zhang, R.J. Microscopic Utilization Characteristics of Nano-Pore Crude Oil During CO_2 Huff and Puff in Shale Oil Reservoirs. *Pet. Explor. Dev.* **2022**, *49*, 557–564. [CrossRef]
22. Li, B.F.; Zheng, L.; Bai, H.; Zhu, D.; Li, Z.M.; Xu, J.G. Characteristics of pore oil utilization in CO_2 huff and puff production of fractured tight reservoirs. *J. China Univ. Pet. (Nat. Sci. Ed.)* **2023**, *47*, 119–127.
23. Liu, J.Y.; Li, M.; Liu, Y.; Zhou, H. Visualization Experiment of Microscopic Mechanism of CO_2 Huff and Puff. *Fault-Block Oil Gas Field* **2017**, *24*, 230–232.
24. ZHao, B.W. A Visual Experimental Study on the Impact of Fractures on CO_2 Flooding in Low Permeability Oil Reservoirs. *Unconv. Oil Gas* **2022**, *9*, 87–93+99.
25. Li, J.; Cheng, B.; Liu, R.; Meng, F.; Liu, Y.; Gao, Y.; Ma, K.; Jiang, H. Microscopic mechanism of water sensitivity of pore-scale sandy conglomerate based on digital core. *Acta Pet. Sin.* **2019**, *40*, 594.

26. Al-Yaseri, A.Z.; Lebedev, M.; Vogt, S.J.; Johns, M.L.; Barifcani, A.; Iglauer, S. Pore-scale analysis of formation damage in Bentheimer sandstone with in-situ NMR and micro-computed tomography experiments. *J. Pet. Sci. Eng.* **2015**, *129*, 48–57. [CrossRef]
27. Enab, K.; Emami-Meybodi, H. Effects of Diffusion, Adsorption, and Hysteresis on Huff-n-Puff Performance in Ultratight Reservoirs with Different Fluid Types and Injection Gases. *Energies* **2021**, *14*, 7379. [CrossRef]
28. Amer, M.W.; Aljariri Alhesan, J.S.; Ghassan, A.L.B. Ultrasonic extraction of oil shale bitumen and study of its structural features using GC-MS and NMR techniques. *Int. J. Coal Prep. Util.* **2023**, *43*, 1524–1541. [CrossRef]
29. Saeed, S.A.; Taura, U.; Al-Wahaibi, Y.; Al-Muntaser, A.A.; Yuan, C.; Varfolomeev, M.A.; Al-Bahry, S.; Joshi, S.; Djimasbe, R.; Suwaid, M.A.; et al. Hydrothermal conversion of oil shale: Synthetic oil generation and micro-scale pore structure change. *Fuel* **2022**, *312*, 122786. [CrossRef]
30. Al-Shalabi, E.W.; Ghosh, B. Flow visualization of fingering phenomenon and its impact on waterflood oil recovery. *J. Pet. Explor. Prod. Technol.* **2018**, *8*, 217–228. [CrossRef]
31. Liu, D.Q. Study on Microscopic Infiltration and "Stuck Well" Production Mechanism of Fracturing Fluid. Master's Thesis, China University of Petroleum, Beijing, China, 2017.
32. Pu, W.F.; Wang, C.Y.; Li, Y.B.; Wei, B.; Jin, F.Y. Nuclear magnetic resonance experimental study of CO_2 flooding in tight reservoir. *Sci. Technol. Eng.* **2017**, *17*, 30–35.
33. Xu, T.; Wang, J.; Lu, Y.; Wang, D.; Yu, L.; Tian, Y. Exploring pore-scale production characteristics of oil shale after CO_2 huff 'n' puff in fractured shale with varied permeability. *Int. J. Coal Sci. Technol.* **2024**, *11*, 12. [CrossRef]
34. Dong, X.; Shen, L.W.; Liu, X.; Zhang, P.; Sun, Y.; Yan, W.; Jiang, L.; Wang, F.; Sun, J. NMR characterization of a tight sand's pore structures and fluid mobility: An experimental investigation for CO_2 EOR potential. *Mar. Pet. Geol.* **2020**, *118*, 104460. [CrossRef]
35. Liu, Y.; Yao, Y.; Liu, D.; Zheng, S.; Sun, G.; Chang, Y. Shale pore size classification: An NMR fluid typing method. *Mar. Pet. Geol.* **2018**, *96*, 591–601. [CrossRef]
36. Yang, K.; Yang, S.L.; Liu, X.Y.; Chen, J.; Yu, J. Study on microscopic development characteristics and influencing factors of nanopores during CO2 huff-puff in Lucaogou Formation shale oil reservoir. In Proceedings of the 15th International Conference on Applied Energy, Doha, Qatar, 3–7 December 2023.